6394 *Biochemistry* **2010,** *49,* 6394–6399
DOI: 10.1021/bi1007645

BIOCHEMISTRY
including biophysical chemistry & molecular biology
Article

Structural and Kinetic Study of the Extended Active Site for Proton Transfer in Human Carbonic Anhydrase II[†]

John F. Domsic,[‡,§] Wilton Williams,[‡] Suzanne Z. Fisher,[‡,∥] Chingkuang Tu,[⊥] Mavis Agbandje-McKenna,[‡] David N. Silverman,*[,‡,⊥] and Robert McKenna*[,‡]

[‡]*Department of Biochemistry and Molecular Biology and* [⊥]*Department of Pharmacology and Therapeutics, University of Florida, Gainesville, Florida 32610.* [§]*Current address: The Wistar Institute, Philadelphia, PA 19104.* [∥]*Current address: Bioscience Division MS M888, Los Alamos National Laboratory, Los Alamos, NM 87545*

Received May 13, 2010; Revised Manuscript Received June 23, 2010

ABSTRACT: The catalysis of CO_2 hydration by human carbonic anhydrase II (HCA II) is limited in maximal velocity by proton transfer from a zinc-bound water molecule to the proton shuttle His64. This proton transfer occurs along a hydrogen-bonded water network, leading to the proton shuttle residue His64, which in turn transfers the proton to bulk solvent. The side chain of His64 occupies two conformations in wild-type HCA II, pointing inward toward the zinc or outward toward bulk solvent. Previously, several studies have examined the roles of residues of the active site cavity that interact with the solvent-mediated hydrogen-bonded network between His64 and the zinc-bound water. Here these studies are extended to examine the effects on proton transfer by mutation at Lys170 (to Ala, Asp, Glu, and His), a residue located near the side chain of His64 but over 15 Å away from the active site zinc. In all four variants, His64 is observed in the inward conformation associated with a decrease in the pK_a of His64 by as much as 1.0 unit and an increase in the rate constant for proton transfer to as much as 4 μs^{-1}, approximately 5-fold larger than wild-type HCA II. The results show a significant extension of the effective active site of HCA II from the zinc-bound water at the base of the conical cavity in the enzyme to Lys170 near the rim of the cavity. These data emphasize that the active site of HCA II is extended to include residues that, at first glance, appear to be too far from the zinc to exert any catalytic effects.

The carbonic anhydrases (CAs) catalyze the hydration of CO_2 to produce bicarbonate and a proton. This catalysis involves two separate and distinct stages. One is the reaction of CO_2 with the zinc-bound hydroxide of the enzyme, yielding bicarbonate and leaving a water molecule at the zinc (eq 1). The other is the regeneration of the zinc-bound hydroxide by the transfer of a proton to bulk solution (eq 2).

$$CO_2 + EZnOH^- \rightleftharpoons EZnHCO_3^- \overset{H_2O}{\rightleftharpoons} EZnH_2O + HCO_3^- \quad (1)$$

$$\begin{aligned} His64-EZnH_2O + B &\rightleftharpoons H^+His64-EZnOH^- + B \\ &\rightleftharpoons His64-EZnOH^- + BH^+ \end{aligned} \quad (2)$$

Here, B is an exogenous proton acceptor from solution, and H^+ shown before His64 in eq 2 represents a protonated site on the enzyme. The rate-determining step for maximum velocity in catalysis by human carbonic anhydrase II (HCA II)[1] in the presence of adequate buffer is the intramoleclular proton transfer of eq 2. In this stage the proton is transferred via a hydrogen-bonded network of water molecules to the solvent-accessible residue His64, which transfers the proton to bulk solvent (*1*, *2*).

The side chain of His64 in crystal structures of HCA II is found in two orientations, inward, pointing toward the proton wire, and outward, pointing toward bulk solution (*3*−*5*). This orientation is somewhat pH dependent with the inward orientation favored at high pH and the outward at low pH (*4*). The availability of these two conformational states has been suggested as promoting the efficient proton transfer of catalysis (*6*, *7*), although this issue is not settled (*8*). Moreover, it has been found that the orientation of His64 is quite sensitive to residues that line the conical cavity. The replacement of Thr200 in HCA II with serine, some 5 Å distant from His64, altered the conformation of the side chain of His64 predominantly to the outward orientation (*9*). In addition, the replacement of Tyr7 in this cavity caused the side chain of His64 to be predominantly in the inward orientation (*10*).

To determine whether the properties of His64 are sensitive to residues near the surface of the protein, that is on the distal side of residue 64, Lys170 has been investigated. This residue lies in a basic patch of amino acids (Lys168, Lys170, and Lys172) on the surface of HCA II (Figure 1A). The side chain amino group of Lys170 is ~6 Å from $N^{\varepsilon 2}$ of His64 in the outward orientation and 15 Å from the zinc at the active site (Figure 1). Moreover, this residue is conserved in CA II from species as diverse as chicken, rat, and bovine (*11*). In this structure−function study using X-ray crystallography and kinetic methods, we report that replacement of Lys170 altered the orientation of the side chain of His64 and decreased its pK_a. In addition, site-specific variants at residue 170 had increased rate constants for proton transfer in the catalyzed dehydration of bicarbonate. This shows that the effective active site of HCA II extends to a region of the conical cavity quite distant from the zinc and close to the exterior of the enzyme.

[†]This work was supported by a grant from the NIH (GM 25154).
*To whom correspondence should be addressed. R.M.: phone, 352-392-5696; fax, 352-392-3422; e-mail, rmckenna@ufl.edu. D.N.S.: phone, (352) 392 3556; fax, (352) 392 9696; e-mail, silvrmn@ufl.edu..
[1]Abbreviation: HCA II, human carbonic anhydrase II.

 Published on Web 06/25/2010

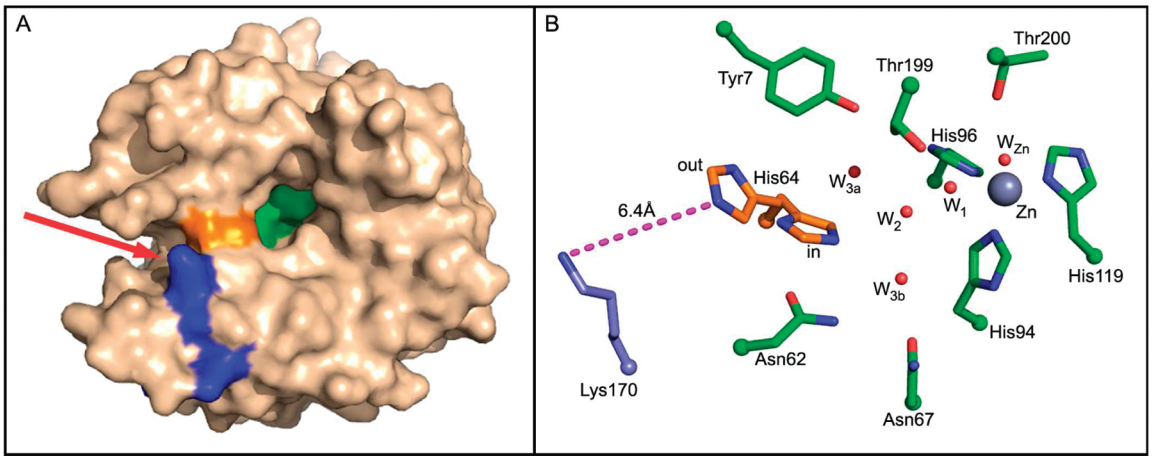

FIGURE 1: Crystal structure of the active site of wild-type HCA II showing the position of Lys170 and His64 (PDB ID 1tbt (*5*)). (A) Surface representation of HCA II showing the relative locations of the active site (green), His64 (orange), and the basic patch of lysines (blue), with Lys170 indicated by the red arrow. (B) Detailed view of the active site showing the location of the solvent proton wire (red spheres) and relevant side chains. The red, dashed line indicates the distance between Lys170 (blue) and His64 (orange). The side chain of His64 is shown in the inward and outward orientations.

MATERIALS AND METHODS

Site-Directed Mutagenesis and Purification. Variants of HCA II were generated using the QuikChange site-directed mutagenesis kit (Stratagene, La Jolla, CA) and a plasmid vector containing the HCA II coding region. Mutations were verified by sequencing of the entire HCA II coding region. Plasmids were then transformed into *Escherichia coli* BL21(DE3)pLysS expression cells. The lysate was run on a preequilibrated column consisting of an agarose matrix conjugated to *p*-(aminomethyl)-benzenesulfonamide (*12*). HCA II variants were eluted with 0.1 M Tris-HCl and 0.4 M sodium azide, pH 7.0. After extensive buffer exchange against 15 mM Tris-HCl, pH 8.0, the samples were concentrated to approximately 10 mg/mL as measured by UV spectroscopy (ε = 54800 M^{-1} cm^{-1}). SDS−PAGE followed by Coomassie staining was used to verify greater than 95% purity of the sample.

^{18}O Exchange. This technique measures the depletion of ^{18}O from species of CO_2 measured via membrane inlet mass spectrometry (*13*). The CO_2 passing across a silicon rubber membrane enters a mass spectrometer (Extrel EXM-200), thus providing a continuous measure of the isotopic content of the CO_2. The dehydration of the labeled bicarbonate has a probability of transiently labeling the active site zinc with ^{18}O (eq 3). The subsequent protonation the zinc-bound hydroxide produces $H_2{}^{18}O$, which is then released into bulk solvent (eq 4).

$$\mathrm{HCOO^{18}O^-} + \mathrm{EZnH_2O} \leftrightarrows \mathrm{EZnHCOO^{18}O} \leftrightarrows \mathrm{COO} + \mathrm{EZn^{18}OH^-} \quad (3)$$

$$\mathrm{H^+His64-EZn^{18}OH^-} \leftrightarrows \mathrm{His64-EZnH_2{}^{18}O} \leftrightarrows \mathrm{His64-EZnH_2O} + \mathrm{H_2{}^{18}O} \quad (4)$$

This method provides two rates for CA-catalyzed ^{18}O exchange. The first is R_1, the rate of exchange of CO_2 and HCO_3^- at chemical equilibrium.

$$R_1/[\mathrm{E}] = k^{\mathrm{ex}}{}_{cat}[\mathrm{S}]/(K^{\mathrm{s}}{}_{eff}[\mathrm{S}]) \quad (5)$$

In eq 5, $k^{\mathrm{ex}}{}_{\mathrm{cat}}$ is the rate constant for the maximal interconversion of substrate and product, $K^{\mathrm{S}}{}_{\mathrm{eff}}$ is the apparent binding constant for substrate to enzyme, and [S] is the concentration of substrate, either carbon dioxide or bicarbonate. The ratio $k^{\mathrm{ex}}{}_{\mathrm{cat}}/K^{\mathrm{S}}{}_{\mathrm{eff}}$ is, in theory and in practice, is equal to $k_{\mathrm{cat}}/K_{\mathrm{m}}$ obtained by steady-state methods.

The second rate obtained, R_{H_2O}, is the rate of release from the active site of water that bears ^{18}O. It is this component of ^{18}O exchange that is dependent on the donation of protons to the ^{18}O-labeled zinc-bound hydroxide (eq 4).

$$R_{H_2O}/[\mathrm{E}] = k_B/([1 + (K_a)_{\mathrm{donor}}/[\mathrm{H^+}]][1 + [\mathrm{H^+}]/(K_a)_{ZnH_2O}]) \quad (6)$$

The value of this rate R_{H_2O} can be interpreted in terms of the rate constant for proton transfer from the proton donor to the zinc-bound hydroxide according to eq 6. In this equation, k_B is the rate constant for proton transfer and $(K_a)_{\mathrm{donor}}$ and $(K_a)_{ZnH_2O}$ are the ionization constants of the proton donor, predominantly His64 in these experiments, and zinc-bound water. To determine the kinetic constant k_B and the ionization constants, nonlinear least-squares methods were used in the program Enzfitter (Biosoft) to fit eq 6 to pH profiles of $R_{H_2O}/[\mathrm{E}]$.

The measurements for HCA II-catalyzed and uncatalyzed ^{18}O exchange were made at 25 °C in the presence of a total substrate concentration (all species of CO_2) of 25 mM. Additionally, the total ionic strength of solution was kept at 0.2 M by the addition of sodium sulfate.

Esterase Activity. To correctly assign values of pK_a obtained from ^{18}O exchange, another kinetic assay was performed, which allows assignment of the pK_a of the zinc-bound solvent. The CAs in the α class possess the ability to hydrolyze ester linkages, although there is no known physiological role for this activity (*14*). To measure this activity, the hydrolysis of 4-nitrophenyl acetate was monitored by UV spectroscopy at 348 nm, the isosbestic point of 4-nitrophenol and its conjugate base, nitrophenylate anion (ε = 5000 M^{-1} cm^{-1}) (*15*).

Stopped-Flow Spectrophotometry. To measure initial rates of CO_2 hydration, the change in absorbance of a pH indicator was followed using the Applied Photophysics (SX.18MV) stopped-flow spectrophotometer (*16*). Briefly, pH indicator−buffer pairs were used over a pH range from 6.1 to 9.3. Reaction conditions were 25 mM buffer concentration with 0.2 M sodium sulfate and initial CO_2 concentrations ranging from 0.7 to 14 mM. The initial rates were obtained from the first 10% of the reaction, and the kinetic constants k_{cat} and $k_{\mathrm{cat}}/K_{\mathrm{m}}$ were determined from nonlinear least-squares fits of the data (Enzfitter, Biosoft).

Table 1: Data Collection and Refinement Statistics for the Lys170 Variant Structures of HCA II

	K170A	K170D	K170E	K170H
PDB accession no.	3mnh	3mni	3mnj	3mnk
space group	$P2_1$	$P2_1$	$P2_1$	$P2_1$
cell dimensions				
a, *b*, *c* (Å)	42.6, 41.6, 72.8	42.6, 41.6, 72.8	42.6, 41.5, 72.7	42.7, 41.6, 72.8
β (deg)	104.5	104.4	104.4	104.5
resolution (Å)	50−1.65 (1.71−1.65) [d]	50−1.75 (1.81−1.75)	50−1.75 (1.81−1.75)	50−1.75 (1.81−1.75)
R_{sym} [a] (%)	6.9 (41.4)	6.2 (38.7)	6.7 (38.8)	5.4 (32.3)
$I/(\sigma)I$	12.5 (2.1)	20.7 (2.4)	16.4 (2.3)	19.0 (3.3)
completeness	98.4 (98.1)	92.2 (80.9)	93.1 (80.4)	92.7 (80.9)
redundancy	2.7 (2.6)	3.2 (3.0)	3.1 (2.8)	3.2 (3.1)
R_{cryst} [b]/R_{free} [c] (%)	16.8/19.7	16.6/19.8	16.9/20.3	16.3/19.5
no. of atoms (protein/solvent)	2076/139	2071/101	2075/84	2081/102
B-factors (Å^2) (main chain/side chain/solvent)	14.9/17.5/29.2	14.8/17.4/26.7	15.7/17.1/26.4	15.3/18.1/27.3
rmsd bond lengths (Å)/angles (deg)	0.011/1.299	0.012/1.361	0.013/1.388	0.012/1.334
Ramachandran statistics (%), most favored, additionally allowed, generously allowed	88.9, 10.6, 0.5	88.9, 10.6, 0.5	88.9, 10.6, 0.5	88.9, 10.6, 0.5

[a] $R_{sym} = (\sum|I - \langle I\rangle|/\sum\langle I\rangle) \times 100$. [b] $R_{cryst} = (\sum||F_o| - |F_c||/\sum|F_o|) \times 100$. [c] R_{free} is calculated in same manner as R_{cryst}, except that it uses 5% of the reflection data omitted from refinement. [d] Values in parentheses represent highest resolution bin.

Crystallization and Data Collection. Crystals of the HCA II variants were grown under standard conditions (15 mg/mL of protein,1.4 M sodium citrate, 100 mM Tris-HCl, pH 8.5) using the hanging-drop vapor-diffusion technique (*10*). Crystals approximately 1.0 × 0.5 × 0.25 mm^3 appeared after 2−3 days. The crystals were then sealed in quartz capillaries containing a small amount of mother liquor. Diffraction data were collected in-house at room temperature using an R-AXIS IV^{++} image plate system with osmic mirrors and a Rigaku RU-H3R Cu rotating anode operating at 50 kV and 100 mA. The crystal−detector distance was set at 100 mm.

Data Processing and Refinement. Diffraction data were indexed, integrated, and scaled using the HKL2000 program package (*17*). Final statistics were similar for the four variants (Table 1). Model refinement was accomplished using the REFMAC5 in the CCP4 suite of programs (*18*) with the 1.54 Å resolution structure of wild-type HCA II (PDB ID: 1tbt (*5*)) with both Lys170 and His64 mutated to Ala to avoid model bias and the zinc, alternate conformations, and all solvent molecules removed. After an initial round of rigid-body fitting, simulated annealing to 3000 K was carried out using CNS (*19*). Energy minimization, *B*-factor refinement, and electron density map generation followed. After the first round, the zinc ion was placed in the active site, and side chains were manually refined as needed using the molecular graphics program Coot (*20*). It was noted that, even after several rounds of refinement, no density was visible for the outward conformation of His64. Waters were then placed and confirmed in Coot during several rounds of refinement until the R_{cryst} reached convergence. Final refinement statistics for all four variants are given in Table 1. Final models and structure factors were submitted to the Protein Data Bank (http://www.pdb.org) with the following accession codes: 3mnh (K170A), 3mni (K170D), 3mnj (K170E), and 3mnk (K170H).

RESULTS

Catalysis. Catalysis by site-specific variants of HCA II with replacements of Lys170 was measured by the exchange of ^{18}O between CO_2 and water. Values of $k^{ex}_{cat}/K^{CO_2}_{eff}$ were obtained by a fit of eq 5 (with substrate S as CO_2) to the data. The pH profiles of $k^{ex}_{cat}/K^{CO_2}_{eff}$ for the hydration of CO_2 were closely superimposable with each other and with wild-type HCA II (Figure 2,

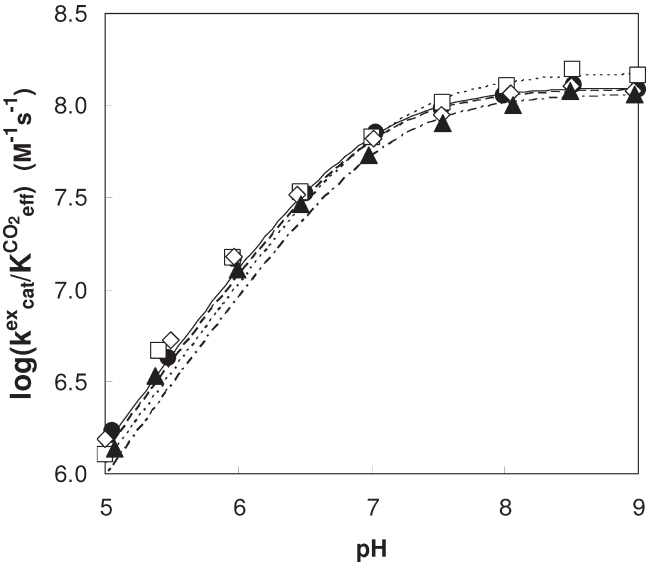

FIGURE 2: pH dependence of $k^{ex}_{cat}/K^{CO_2}_{eff}$ (M^{-1} s^{-1}) for the hydration of CO_2 catalyzed by the following variants of HCA II: (▲) K170A; (◇) K170D; (□) K107E; and (●) K170H. Lines were obtained by a fit of eq 5 to ^{18}O exchange data with constants given in Table 2. Solutions at 25 °C contained 25 mM of all species of CO_2. Ionic strength was maintained at 0.2 M by addition of sodium sulfate. No buffers were used.

Table 2). This was expected since the side chain of the replaced Lys170 is far from the zinc at the active site; the distance from the N^{ζ} of Lys170 to the zinc is about 15 Å (*5*). These data were fit to a single ionization, the pK_a of which is an estimate of the ionization of the zinc-bound water (*21*). For each of the variants at residue 170 the pK_a was found to be very close to 7 for the zinc-bound water, unchanged compared to wild-type HCA II (Table 2). These values of pK_a were confirmed by a second independent measurement of the pK_a of the zinc-bound water obtained from the pH profile of k_{cat}/K_m for the hydrolysis of 4-nitrophenyl acetate (Table 3). These data confirm that the pK_a close to 7 of the zinc-bound water was unchanged in the variants of Tables 2 and 3.

On the other hand, the values of the proton transfer dependent rate of release of $H_2{}^{18}O$ from the enzyme R_{H_2O}/[E] were clearly perturbed for each of the variants, as shown by the superimposed pH profiles given in Figure 3. These data indicate that the rates of

Table 2: Apparent Values of pK_a and Maximal Rate Constants for Kinetic Measurements of Catalysis by Wild-Type and Site-Specific Variants of HCA II at Residue 170 Obtained by ^{18}O Exchange at 25 °C[a]

	from R_{H_2O}		from R_1	
	pK_a (His64)[b]	k_B (μs^{-1})[b]	pK_a (ZnH_2O)	$K^{ex}_{cat}/K^{CO_2}_{eff}$ (μM^{-1} s^{-1})
wild type	7.2 ± 0.1	0.8 ± 0.1	6.9	100
K170A	6.7 ± 0.1	1.2 ± 0.1	7.0	110
K170D	6.7 ± 0.1	1.5 ± 0.2	7.0	120
K170E	6.3 ± 0.1	4.0 ± 0.4	7.1	150
K170H	6.7 ± 0.1	1.6 ± 0.1	6.9	120

[a]Solutions contained 25 mM of all species of CO_2 at sufficient sodium sulfate to maintain ionic strength at 0.2 M. No buffers were added. Data were obtained by fits of eq 5 for R_1 and eq 6 for R_{H_2O} to data shown in Figures 2 and 3. [b]These values were obtained by a least-squares fit of the data of Figure 3 to eq 6.

Table 3: Values of pK_a for Zinc-Bound Water and Maximal Value of k_{cat}/K_m for Catalysis of Hydrolysis of 4-Nitrophenyl Acetate by Variants of HCA II at 25 °C

	pK_a (ZnH_2O)	k_{cat}/K_m (M^{-1} s^{-1})
wild type	7.0	2800
K170A	7.0	1600
K170D	7.1	1850
K170E	6.9	1890
K170H	6.9	1760

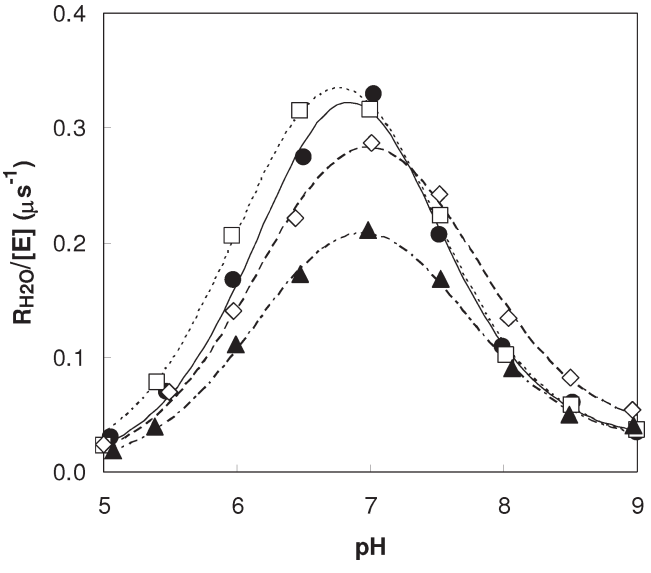

FIGURE 3: pH dependence of $R_{H_2O}/[E]$ (μs^{-1}), the rate constant for the release of $H_2{}^{18}O$ from the enzyme catalyzed by the following variants of HCA II: (▲) K170A; (◇) K170D; (□) K107E; and (●) K170H. The lines are a fit of eq 6 to the data with constants given in Table 2. Conditions were as described for Figure 2.

proton transfer between His64 and the zinc-bound hydroxide and/or their pK_a values have been affected by the replacements at residue 170. The lines in Figure 3 are fits of eq 6 to the data with values of apparent pK_a for proton donor (His64) and acceptor and derived rate constant for proton transfer k_B given in Table 2. There are two prominent solutions of eq 6 in best fits to the data for each variant of Figure 3. An interchange of the values of the pK_a of the zinc-bound water and the pK_a of His64 both provide satisfactory convergence of eq 6 to the data. However, the pK_a of the zinc-bound water appears to be firmly established from both ^{18}O exchange and ester hydrolysis and assigned appropriately.

The data of Table 2 show two general trends. One trend is that the apparent pK_a of the predominant proton donor His64 appears lower in the variants than for wild type (Table 2). The apparent pK_a for His64 estimated from ^{18}O exchange data appears between 6.3 and 6.7 for the variants of Table 2, lower than the value of 7.2 estimated for wild-type HCA II. A second trend for the variants was an increased value of k_B, the rate constant for proton transfer in the dehydration direction obtained from ^{18}O exchange results. This value is 0.8 μs^{-1} for wild-type HCA II (*10*, *22*). Although the propagated uncertainty in the values of k_B can be large (as great as 13% in Table 2), it is clear from the data that k_B was increased for each of the variants. It is interesting that the rate constant for proton transfer k_B for K170H HCA II was similar to that for K170A. The Ala residue at 170 is not capable of proton transfer; hence, the data suggest that His170 is not significantly involved as a proton shuttle.

These data on catalysis were compared to data obtained at steady state by stopped-flow spectrophotometry. The bicarbonate dehydration kinetics of K170A HCA II were measured at pH 5.8 and 6.0. Deviations from Michaelis−Menten behavior were observed, and steady-state rate constants could not be obtained. In the CO_2 hydration direction, catalysis by K170A HCA II was adequately described by Michaelis−Menten kinetics with maximal values of k_{cat} = (0.50 ± 0.04) μs^{-1} and k_{cat}/K_m = (100 ± 10) μM^{-1} s^{-1}.

Crystallography. The crystal structures of the four variants K170A, K170D, K170E, and K170H HCA II were solved to between 1.65 and 1.75 Å resolution with final R_{crysts} of ~16.5% and R_{frees} ~20% (Table 1). Overall, no major structural perturbations were observed with C^α rmsd of approximately 0.09 Å for all four variants when compared to wild-type HCA II. The hydrogen-bonded solvent network in the active site cavity was conserved in all four structures, indicating that the replacements at residue 170 had not affected this aspect of active site structure. A large electron density peak was noticed near the side chains of His64, Asn62, and Asn67 and was modeled as a sodium ion, as the placement of a water molecule could not account for the entirety of the observed density. However, the exact identity of this atom is not clear from crystallographic analysis as the resolution of the structures and the possibility of partial occupancy of this atom preclude an absolute determination of the atom type.

The proton shuttle residue, His64, which occupies two conformations in wild-type HCA II (*4*, *23*), was observed only in the inward conformation in all four variants. Additionally, in these four variants, there was a change in the occupancy and position of residues His3 and His4. Typically at this resolution, electron densities for His3 and His4 are not observed due to the inherent disorder of the N-terminus of wild-type HCA II. In the four variants of Table 2, distinct electron density was observed for His3 and His4, showing that these residues occupy a conformation that is distinct from previous structures that have been reported for these residues (*5*, *23*) (Figure 4, Supporting Information Figure S1). This is most clear for His4 for which electron densities appear for the entire side chain in each of the four variants and not as clear for His3 in which electron densities are less complete except for K170D (Figure 4). The position of these residues is such that the side chain of His3 is located near what would be the outward conformation of His64 (Figure 5A). A small amount of additional density was observed extending off of the backbone of His3; however, it was not modeled as it does not cover an entire residue.

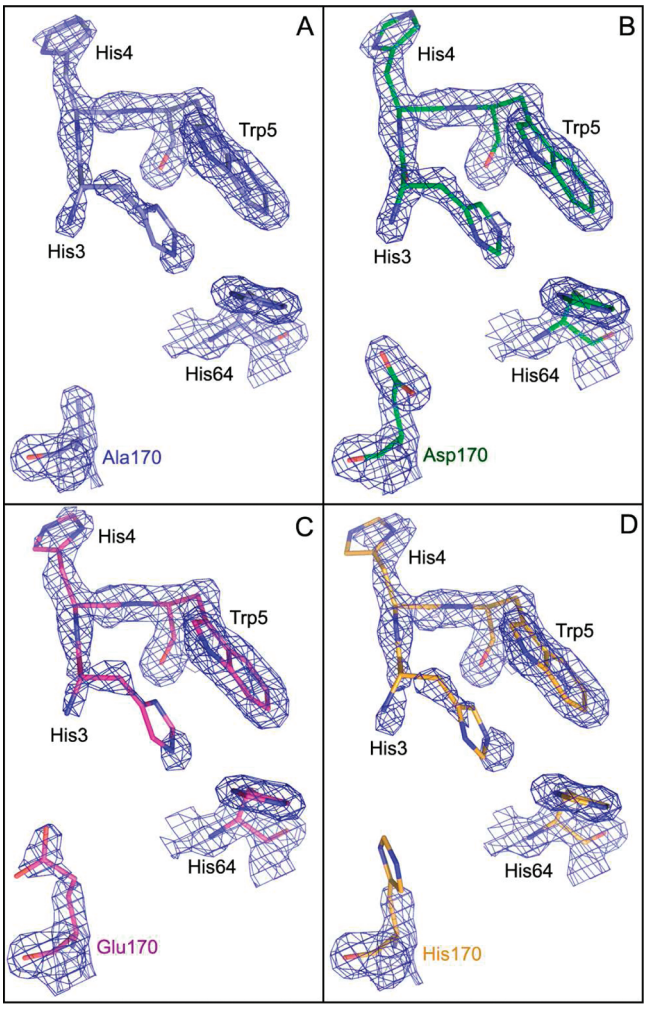

FIGURE 4: Electron density for His3 and His4 as seen in all four variants at position 170: (A) K170A; (B) K170D; (C) K170E; and (D) K170H. The level of electron density varies between the four structures and is the highest for K170D (B). Density maps shown are $F_o - F_c$ maps contoured at 1.5σ.

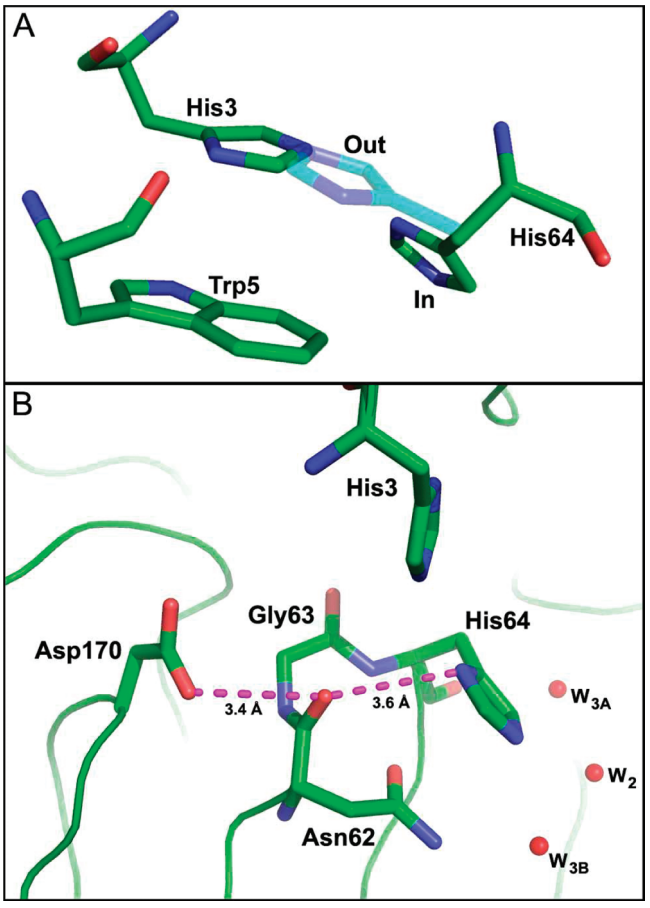

FIGURE 5: (A) The side chain of His3 overlaps with the typical position of the outward conformation of His64 in wild-type HCA II. (B) The carboxylate of Asp170 in K170D is within hydrogen-bonding distance of the backbone carbonyl of Asn62, which in turn can form a hydrogen bond with His64 in the inward orientation.

DISCUSSION

It is apparent that the replacement of Lys170 has caused changes in three prominent properties of the proton shuttle residue His64: its orientation within the active site cavity, its pK_a, and the rate constant for proton transfer from His64 to the zinc-bound hydroxide in catalysis. In all four variants examined here, the side chain of His64 exists predominantly in the inward conformation in contrast with the wild-type HCA II which shows both orientations in crystal structures. Interestingly, the inward orientation of His64 is apparently stabilized by the side chain of His3. Typically in crystal structures of HCA II at this resolution, His3 and His4 are not able to be placed in any electron density due to the inherent flexibility of the N-terminus. In the structures of all four Lys170 variants, the side chain of His3 is seen to apparently π-stack with Trp5, in a position that would overlap the outward conformation of His64 (Figure 5A). Of note are the differences in the levels of electron density around His3 in the four variants. The highest level of electron density is seen in K170D, where the side chain of Asp170 interacts with the backbone carbonyl oxygen of Asn62 (distance = 3.2 Å). In turn, this carbonyl oxygen appears to interact with the $N^{\delta 1}$ atom of His64 (Figure 5B). However, this interaction is only seen in this variant and thus does not fully explain the pK_a effects of the Lys170 mutations. Moreover, K170D, the variant with the highest electron density for His3, does not have the most efficient rate constant for proton transfer k_B (Table 2).

The apparent pK_a for His64 in the variants of Table 1 estimated from ^{18}O exchange data is between pK_a 6.3 and 6.7 (Table 2), lower than the value of 7.2 in similar experiments for wild-type HCA II (*10*). This decrease in apparent pK_a for His64 is probably due to the inward orientation of this side chain in each of the variants, an orientation in which it is located in a more hydrophobic environment. This same effect was observed for Y7F HCA II (*10*) and in variants containing replacements of Asn62 with hydrophobic residues (N62A, N62V, N62L) (*24*) in which the orientation of His64 is also in the inward orientation. In these cases the pK_a of His64 was near 6.0.

The rate constants for proton transfer k_B in catalytic dehydration were increased from 0.8 μs^{-1} for wild-type HCA II to 1.2−4.0 μs^{-1} for the variants (Table 2). This effect is not large but represents as much as a 5-fold enhancement of k_B, most likely attributed to the changes in properties of His64 discussed above, specifically the decrease in the pK_a of an inward His64 which makes it a better proton donor in the dehydration direction. This lower value of pK_a also makes it a poorer proton acceptor in the hydration direction, a feature which is supported by the value of k_{cat} = 0.50 μs^{-1} for hydration of CO_2 catalyzed by K170A HCA II. This is lower than the value of k_{cat} = 1.0 μs^{-1} for hydration catalyzed by wild type (*16*).

These explanations are amplified in the more complex analysis provided by computational simulations. Multistate empirical valence bond simulations of Maupin et al. (*25*) show that the side chain of Lys170, among other residues, lies close to the pathway for proton transfer with His64 in the outward orientation. These studies indicate a higher energy barrier for proton transfer with His64 in the outward compared with inward orientations, due in large part to larger water clusters associated with the outward state. However, combined quantum mechanical/molecular mechanical simulations of Riccardi et al. (*26*) emphasize electrostatics and suggest that the inward orientation of His64 offers no advantage in rate constants for proton transfer compared with the outward.

The decreased pK_a for His64 explains in part why these mutations at residues 7 and 170 do not appear in nature. To maintain maximal activity in both hydration and dehydration directions, it is necessary that the values of pK_a for the proton donor and acceptor be closely matched, as they are in HCA II. This allows the enzyme to function efficiently in both hydration and dehydration as required in respiration and in regulation of cellular pH. Thus it appears that one function of Lys170 is to maintain an environment of His64 that maximizes proton transfer and hence catalysis of the hydration of CO_2 and dehydration of bicarbonate. However, this may not describe entirely the function of Lys170. Although Lys170 appears in CA II from chicken, rat, bovine, and humans, all of which have His64, it also appears in CA III and CA V, which do not have a histidine at residue 64 (*11*).

In summary, these results show a significant extension of the effective active site of HCA II from the zinc-bound water at the bottom of the conical cavity in the enzyme to Lys170 about 15 Å from the zinc and near the rim of the cavity. It is now apparent from this and other work (*10*, *24*) that at least four residues in the active site cavity with side chains more than 7 Å from the zinc (Tyr7, Asn62, Asn67, and Lys170) serve to finely tune the proton transfer properties of His64. This also explains in part why nature needs so large an enzyme to catalyze efficiently such a simple reaction as the hydration of CO_2.

SUPPORTING INFORMATION AVAILABLE

A diagram of the conformations of the N-terminal ends of K170A, K170D, K170E, and K170H compared with wild-type HCA II. This material is available free of charge via the Internet at http://pubs.acs.org.

REFERENCES

1. Steiner, H., Jonsson, B. H., and Lindskog, S. (1975) Catalytic mechanism of carbonic-anhydrase—Hydrogen-isotope effects on kinetic-parameters of human C isoenzyme. *Eur. J. Biochem. 59*, 253–259.
2. Tu, C. K., Silverman, D. N., Forsman, C., Jonsson, B. H., and Lindskog, S. (1989) Role of histidine 64 in the catalytic mechanism of human carbonic anhydrase II studied with a site-specific mutant. *Biochemistry 28*, 7913–7918.
3. Liljas, A., Lovgren, S., Bergsten, P. C., Carlbom, U., Petef, M., Waara, I., Strandbe., B, Fridborg, K., Jarup, L., and Kannan, K. K. (1972) Crystal-structure of human carbonic anhydrase-C. *Nat. New Biol. 235*, 131–137.
4. Nair, S. K., and Christianson, D. W. (1991) Unexpected pH-dependent conformation of His-64, the proton shuttle of carbonic anhydrase-II. *J. Am. Chem. Soc. 113*, 9455–9458.
5. Fisher, Z., Hernandez Prada, J. A., Tu, C., Duda, D., Yoshioka, C., An, H., Govindasamy, L., Silverman, D. N., and McKenna, R. (2005) Structural and kinetic characterization of active-site histidine as a proton shuttle in catalysis by human carbonic anhydrase II. *Biochemistry 44*, 1097–1105.
6. Jude, K. M., Wright, S. K., Tu, C., Silverman, D. N., Viola, R. E., and Christianson, D. W. (2002) Crystal structure of F65A/Y131C-methylimidazole carbonic anhydrase V reveals architectural features of an engineered proton shuttle. *Biochemistry 41*, 2485–2491.
7. Silverman, D. N., and McKenna, R. (2007) Solvent-mediated proton transfer in catalysis by carbonic anhydrase. *Acc. Chem. Res. 40*, 669–675.
8. Mikulski, R. L., and Silverman, D. N. (2010) Proton transfer in catalysis and the role of proton shuttles in carbonic anhydrase. *Biochim. Biophys. Acta 1804*, 422–426.
9. Krebs, J. F., Fierke, C. A., Alexander, R. S., and Christianson, D. W. (1991) Conformational mobility of His-64 in the Thr200Ser mutant of human carbonic anhydrase-II. *Biochemistry 30*, 9153–9160.
10. Fisher, S. Z., Tu, C. K., Bhatt, D., Govindasamy, L., Agbandje-McKenna, M., McKenna, R., and Silverman, D. N. (2007) Speeding up proton transfer in a fast enzyme: kinetic and crystallographic studies on the effect of hydrophobic amino acid substitution in the active site of human carbonic anhydrase II. *Biochemistry 42*, 3803–3813.
11. Hewett-Emmett, D., and Tashian, R. E. (1996) Functional diversity, conservation, and convergence in the evolution of the alpha-, beta-, and gamma-carbonic anhydrase gene families. *Mol. Phylogenet. Evol. 5*, 50–77.
12. Khalifah, R. G., Strader, D. J., Bryant, S. H., and Gibson, S. M. (1977) C-13 nuclear magnetic-resonance probe of active-site ionizations in human carbonic-anhydrase B. *Biochemistry 16*, 2241–2247.
13. Silverman, D. N. (1982) Carbonic anhydrase: oxygen-18 exchange catalyzed by an enzyme with rate-contributing proton-transfer steps. *Methods Enzymol. 87*, 732–752.
14. Gould, S. M., and Tawfik, D. S. (2005) Directed evolution of the promiscuous esterase activity of carbonic anhydrase II. *Biochemistry 44*, 5444–5452.
15. Verpoorte, J. A., Mehta, S., and Edsall, J. T. (1967) Esterase activities of human carbonic anhydrases B and C. *J. Biol. Chem. 242*, 4221–4229.
16. Khalifah, R. G. (1971) Carbon dioxide hydration activity of carbonic anhydrase. 1. Stop-flow kinetic studies on native human isoenzyme-B and isoenzyme-C. *J. Biol. Chem. 246*, 2561–2573.
17. Otwinowski, Z., and Minor, W. (1997) Processing of X-ray diffraction data collected in oscillation mode. *Methods Enzymol. 276*, 307–326.
18. Murshudov, G. N., Vagin, A. A., and Dodson, E. J. (1997) Refinement of macromolecular structures by the maximum-likelihood method. *Acta Crystallogr., Sect. D: Biol. Crystallogr. 53*, 240–255.
19. Brunger, A. T., Adams, P. D., Clore, G. M., DeLano, W. L., Gros, P., Grosse-Kunstleve, R. W., Jiang, J. S., Kuszewski, J., Nilges, M., Pannu, N. S., Read, R. J., Rice, L. M., Simonson, T., and Warren, G. L. (1998) Crystallography & NMR system: a new software suite for macromolecular structure determination. *Acta Crystallogr., Sect. D: Biol. Crystallogr. 54*, 905–921.
20. Emsley, P., and Cowtan, K. (2004) Coot: model-building tools for molecular graphics. *Acta Crystallogr., Sect. D: Biol. Crystallogr. 60*, 2126–2132.
21. Lindskog, S. (1997) Structure and mechanism of carbonic anhydrase. *Pharmacol. Ther. 74*, 1–20.
22. Duda, D., Tu, C. K., Qian, M. Z., Laipis, P., Agbandje-McKenna, M., Silverman, D. N., and McKenna, R. (2001) Structural and kinetic analysis of the chemical rescue of the proton transfer function of carbonic anhydrase II. *Biochemistry 40*, 1741–1748.
23. Fisher, S. Z., Maupin, C. M., Budayova-Spano, M., Govindasamy, L., Tu, C., Agbandje-McKenna, M., Silverman, D. N., Voth, G. A., and McKenna, R. (2007) Atomic crystal and molecular dynamics simulation structures of human carbonic anhydrase II: insights into the proton transfer mechanism. *Biochemistry 46*, 2930–2937.
24. Zheng, J. Y., Avvaru, B. S., Tu, C., McKenna, R., and Silverman, D. N. (2008) Role of hydrophilic residues in proton transfer during catalysis by human carbonic anhydrase II. *Biochemistry 47*, 12028–12036.
25. Maupin, C. M., McKenna, R., Silverman, D. N., and Voth, G. A. (2009) Elucidation of the proton transport mechanism in human carbonic anhydrase II. *J. Am. Chem. Soc. 131*, 7598–7608.
26. Riccardi, D., Konig, P., Guo, H., and Cui, Q. (2008) Proton transfer in carbonic anhydrase is controlled by electrostatics rather than the orientation of the acceptor. *Biochemistry 47*, 2369–2378.